

Nanoscale Horizons

XeF2 Gas Assisted Focused Electron Beam Induced Etching of Niobium Thin Films: Towards Direct Write Editing of Niobium Superconducting Devices

Journal:	Nanoscale Horizons			
Manuscript ID	NH-COM-08-2024-000407.R1			
Article Type:	Communication			
Date Submitted by the Author:	07-Oct-2024			
Complete List of Authors:	Gellerup, Branden; University of Tennessee Knoxville College of Engineering, Emery, Reece; University of Tennessee, Department of Material Science and Engineering Randolph, Steven; Oak Ridge National Laboratory Rack, Philip; University of Tennessee, Department of Material Science and Engineering Retterer, Scott; UT-Battelle, LLC, Biosciences and Center for Nanophase Materials Sciences			

SCHOLARONE™ Manuscripts We have explored focused electron beam induced etching (FEBIE) using the XeF₂ gaseous precursor to selectively etch and edit niobium films. We have characterized the etching rate and efficiency as a function beam current, beam energy, dwell time, pattern area and precursor pressure. We show that careful consideration of the relative electron and precursor flux reveals a regime of FEBIE parameters that produce etching yields that are greater than 1 Nb atom/e-. Furthermore, a spontaneous etching component emerges, which has implications for larger area etching. We demonstrate that an etch resolution of ~ 17 nm can be achieved via judicious selecting of the FEBIE parameters, which is below the superconducting coherence length of Nb. Thus FEBIE should be an interesting route towards direct write editing of Josephson junctions. Traditional focused ion beam modification methods have been used to process niobium superconducting devices, however, ion beams significantly alter both the morphology and near-surface structure via knock-on collisions during the sputtering process. Furthermore, the milling/etching resolution to date has only demonstrated ~ 65nm resolution for Nb superconducting junctions using a liquid gallium source focused ion beam. Thus, FEBIE presents a promising path forward for low-damage nanoscale synthesis of niobium superconducting applications.

Nanoscale Horizons Page 2 of 25

XeF₂ Gas Assisted Focused Electron Beam Induced Etching of Niobium Thin Films: Towards

Direct Write Editing of Niobium Superconducting Devices

Spencer Gellerup¹, Reece Emery¹, Scott T. Retterer², Steven Randolph^{2*}, Philip D. Rack^{1**}

¹Department of Material Science and Engineering, University of Tennessee – Knoxville,

Knoxville, TN 37996, USA

²Center for Nanophase Materials Science, Oak Ridge National Laboratory, Oak Ridge, TN 37830,

USA

*randolphsj@ornl.gov

**prack@utk.edu

Abstract

In this work, we explore focused electron beam induced etching (FEBIE) of niobium thin films with the XeF₂ precursor as a route to edit, on-the-fly, superconducting devices. We report the effect of XeF₂ pressure, electron beam current, beam energy, and dwell time on the Nb etch rate. To understand the mass transport and reaction rate limiting mechanisms, we compare the relative electron and XeF₂ gas flux and reveal the process is reaction rate limited at low current/short dwell times, but shifts to mass transport limited regimes as both are increased. The electron stimulated etching yield is surprisingly high, up to 3 Nb atoms/electron, and for the range studied has a maximum at 1 keV. It was revealed that spontaneous etching accompanies the electron stimulated process, which was confirmed by varying the etched box size. An optimized etch resolution of 17 nm was achieved. Given that the Nb superconducting coherence length is 38 nm and scales with thickness, this work opens the possibility to direct write Nb superconducting devices via low-damage FEBIE.

1. Introduction

Pure elemental niobium is a type-I superconductor with the highest superconducting transition temp (T_c) for all pure metals, of 9.33 K and upper critical magnetic field (H_{C2}) of 4020 Oe,^[1] where impurities are known to shift the material to a type-II superconductor.^[2] Niobium is also alloyed in superconducting magnets with titanium,^[3] vanadium, ^[4] germanium, ^[5] tin, ^[6] tantalum^[7] and more. Notable types of elemental niobium superconducting devices are used in superconducting radio frequency (SRF) devices,^[8] circuitry and sensors,^[9] qubits,^[10] and field emission microscope tips.^[11] These applications are strongly impacted by the quality of the top few nanometers of the surface, as well as the surface chemistry.^[12] Further, the superconducting properties can be impacted by surface microstructure, as the magnetic flux can be trapped within recrystallized fine-grains between 10-50 mm.^[13] Therefore, to fabricate optimal niobium superconducting nanodevices, a processing method must; i) not disrupt the surface chemistry, ii) be non-destructive to the sample surface/microstructure, and iii) achieve high spatial resolution.

Focused electron beam induced etching (FEBIE) is a nanoscale direct write technique which utilizes an electron beam to dissociate surface-adsorbed precursor gases that react with a film/substrate to form a volatile or non-volatile byproduct. The subsequent desorption (sometimes facilitated via electron stimulated desorption for non-volatile byproducts) leads to the removal of the film/substrate and appropriate beam control leads to on-demand nanoscale etching. This mostly chemical process is contrasted with knock-on sputter removal of material or chemically enhanced sputtering, which are associated with focused ion beam (FIB) milling processes. [14] While convenient for nanoscale material removal, these FIB milling processes can

Nanoscale Horizons Page 4 of 25

induce sub-surface and peripheral damage due to the implanted ions, defect generation, and lattice damage/amorphization associated with the knock-on collisions. Low-energy electron beams (<30 keV) are typically insufficient to generate knock-on events due to the electron's relatively small mass, thus gas mediation from a chemical precursor with FEBIE is required to reach appreciable etching rates. Examples of gaseous precursors used for FEBIE are Cl₂ which has been used to etch chrome oxide,^[15] and nitrosyl chloride (NOCL) which has been used to etch alumina.^[16] XeF₂ is another common vapor phase precursor for both gas-assisted FIB^[17] and FEBIE and has been used with the FEBIE of silicon and silicon dioxide,^[18] silicon nitride,^[19] tantalum nitride,^[20] gallium arsenide,^[21] titanium,^[22-23] chrome,^[24] and recently molybdenum disulfide.^[25] Upon electron stimulation, adsorbed XeF₂ undergoes dissociation via homolytic cleavage that forms fluorine radicals which can be represented by Eq. (1):

$$XeF_2 + e^- \rightarrow Xe + 2F + e^- \tag{1}$$

where the fluorine can react with the material to form volatile fluoride byproducts, which are desorbed and pumped away. One such reaction pathway involving Nb is the generation of volatile niobium pentafluoride as in Eq. (2).^[26-30]

$$5XeF_2 + 5e^- + 2Nb \rightarrow 5Xe + 2NbF_5 + 5e^-$$
 (2)

While the focused primary beam contributes to the reactions in Eq. (1) and (2), consequent secondary and backscattered electrons also participate, and thus the overall process is governed by the precursor mass flow and electron flux and energy distribution at the surface. This method is expected to be successful for many materials that etch in fluorine chemistries,

and given that niobium has been shown to etch in $CBrF_3$ and CF_4 precursors in reactive ion etching (RIE), it was presumed to be an excellent candidate for FEBIE with XeF_2 .^[31]

Fig. 1A) is a simplified schematic of the proposed Nb FEBIE process and Fig. 1B-D) are preliminary etch experiments where we prove the principle of Nb FEBIE. Here we explore the etch rate of superconducting Nb films as a function of electron beam current, dwell time, beam energy, and XeF₂ pressure to optimize the etch rate efficiency of the Nb films. Note, a multiple pass scan strategy was used to achieve the desired etching dose. For optimum current and dwell times, we also explore spatial resolution as a function of beam energy. Finally, we fabricate and test various superconducting structures fabricated via FEBIE.

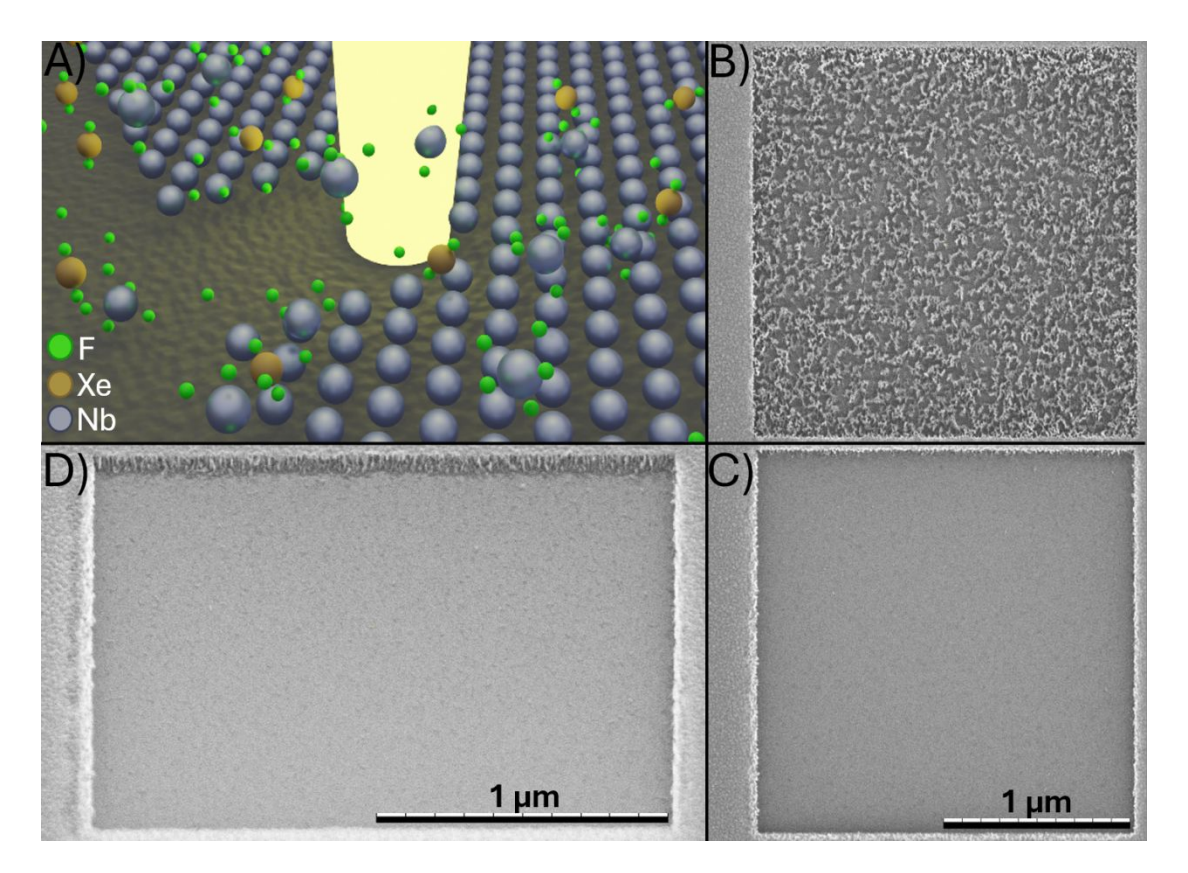


Figure 1. A) Schematic illustrating the focused electron beam induced etching process. B) and C) SEM images illustrate the progression of a 4 μ m² box etched into a Nb film and, D) is a tilted (52°) SEM image of the high-fidelity and anisotropic etch profile.

Nanoscale Horizons Page 6 of 25

2. Material and Methods

Niobium films were magnetron sputtered from a commercial niobium sputtering target (sourced from Kurt J. Lesker, 99.95% purity) after chamber vacuum pressure of 3x10⁻⁷ Torr was achieved. Films were deposited onto a silicon oxide coated silicon wafer where the oxide film conveniently acts as a barrier to spontaneous Si etching once FEBIE of Nb is complete. Argon gas was introduced into the sputter chamber (AJA ATC2400) at the flow rate of 25 sccm at a working pressure of 5 mTorr. A direct current (DC) sputtering power supply delivered a forward power density at the target of 4.9 W/cm² where the Nb target was pre-sputtered for 35 minutes to remove the niobium native oxide on the target surface. Then a 20 minute deposition was performed at a deposition rate of 3.25 nm/min (~65 nm thick film). The Si-SiO₂ wafer on the chamber stage was at a working distance of ~15 cm and was heated to 500°C during the deposition. X-ray diffraction of the Nb film confirmed the expected BCC crystal structure.

FEBIE experiments were conducted within a Thermo Scientific Helios 5 Hydra UX plasma focused ion beam (PFIB), where XeF₂ gas was introduced by a MultiChem™ gas injection system (GIS) positioned at a z-height 238 μm from substrate and from the electron beam field of view.

The crucible of the XeF $_2$ source was cooled to 1°C to reduce the precursor's relatively high vapor pressure. The chamber was allowed to reach a base pressure of approximately $7x10^{-7}$ Torr prior to experimentation. The specific parameters for each experiment are specified in the results section, and also summarized in **Table I**. The XeF $_2$ gas flow was varied by changing the duty cycle of the electronically controlled, pulse width modulated valve from \sim 0.34-1.1% resulting in working chamber pressures of $4.7x10^{-6}$ - $3x10^{-5}$ Torr. The FEBIE patterning conditions used were 0.25-64 μ m 2 area boxes with a constant pixel pitch of 10 nm, dwell times between

0.025- $10~\mu s$, varied electron beam energies between 0.5-20~keV, and beam currents between 0.025-1.6~nA. FEBIE line patterns were $2~\mu m$ long, had a constant pixel pitch of 10~nm, single pixel linewidth, a XeF_2 gas flow duty cycle of ~0.9%, , a beam current of 0.1~nA (which results in an electron beam diameter of 4.4~nm), and varied beam energy and dwell time to test the resolution capabilities of the XeF_2 gas assisted FEBIE process.

The localized average gas flux was estimated by projecting the area of the 500 μ m diameter gas injection nozzle to the substrate. Based on previous capillary flow measurements of various gases, ^[32-34] we assumed that ~44% of the gas emanating from the nozzle is contained within a spread angle of 15°. The XeF₂ flow rate was calculated assuming an effective pumping speed of 234 liter per minute and the steady state chamber pressure realized in the system. The equilibrium XeF₂ flux on the chamber surfaces far away from the nozzle was estimated by the working chamber pressure and kinetic theory of gases. Finally, the effective localized precursor flux enhancement factor of ~1,485 was estimated by taking the ratio of the average gas flux contained within the projected area of the nozzle to the equilibrium gas flux. **Table SI** includes the equilibrium gas flux for each experimental condition.

Etch depths were initially measured by tapping mode atomic force microscopy (AFM) on an Asylum MFP-3D Infinity AFM. AFM and SEM images were correlated such that end-point monitor graphs (EPM) could be used to determine the dose-to-clear (all Nb removed down to SiO_2 layer) for various conditions.

Nanoscale Horizons Page 8 of 25

3. Results

3.1 Box etches

Initially, the effect of varying beam current on the etch rate and efficiency of the gas-assisted FEBIE were investigated using box mode patterning with constant beam energy of 1 keV, single pixel dwell time of 1 μ s, pixel pitch of 10 nm, and XeF₂ working pressure of 1x10⁻⁵ Torr. Etches were conducted for beam currents ranging from 0.025-0.8 nA, then AFM topographic images of etched regions were measured to determine etch depth. **Figure 2A-B)** shows a series of SEM and AFM images of Nb FEBIE box etches performed at 0.025 nA in **Fig. 2A)** and 0.1 nA **Fig. 2B)** and common areal electron doses (nC/ μ m²) labeled above the SEM images (i.e. the 0.025 nA current doses were 4x time).

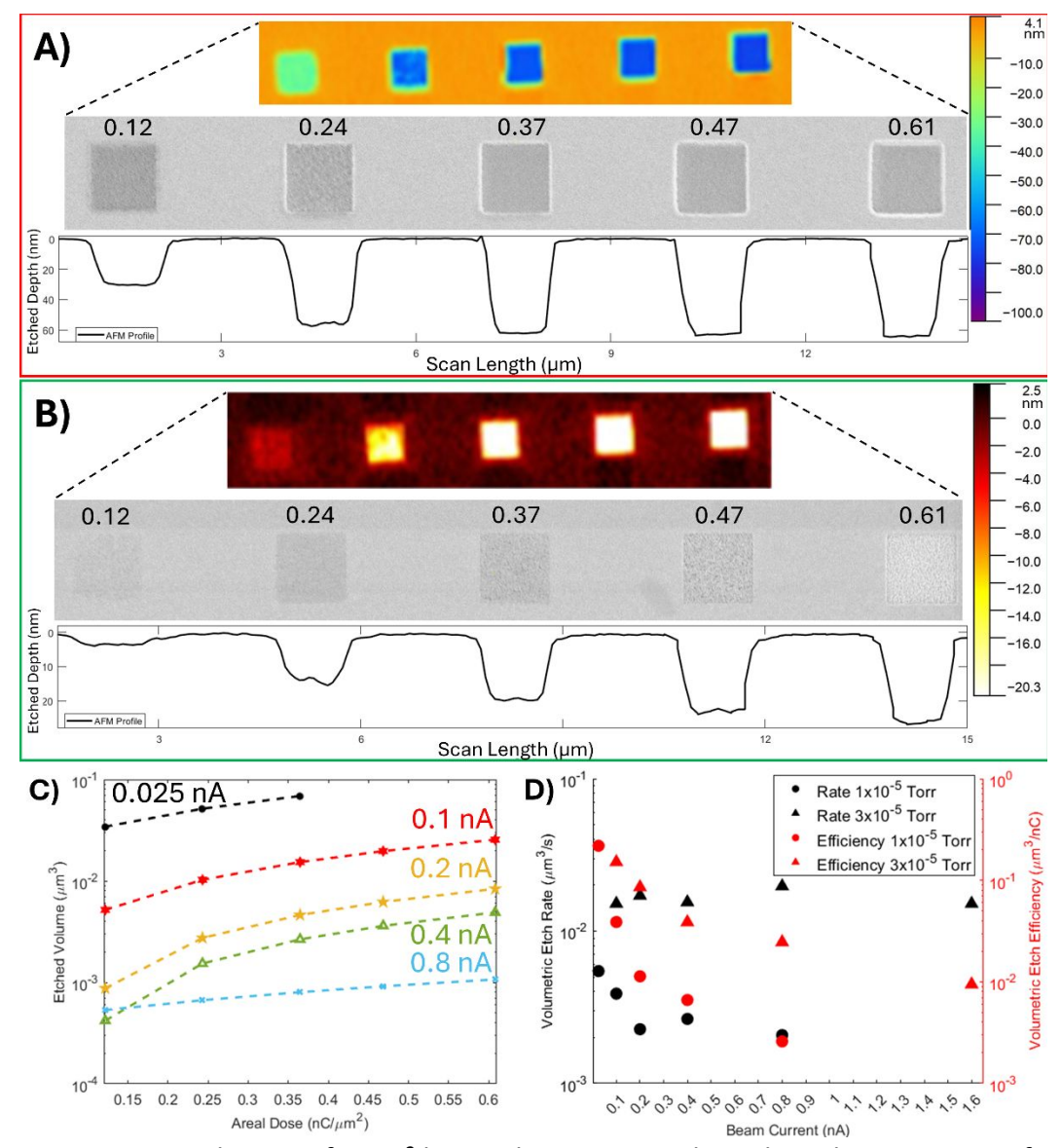


Figure 2. Gas-assisted FEBIE of 1 μ m² box etches were conducted at a beam energy of 1 keV, dwell time of 1 μ s, pixel pitch of 10 nm, XeF₂ working pressure of 1x10⁻⁵ Torr, varying beam currents from 0.025 – 0.8 nA where A) SEM images are correlated with AFM images and line profiles for beam current of 0.025 nA, B) 0.1 nA box series, C) a graph of etched volume per electron dose for various beam currents, and D) plots of FEBIE etch rate (left y-axis) and etch efficiency (right y-axis) versus beam current with data added from XeF₂ working pressures of $3x10^{-5}$ Torr.

As noted, the 0.025 nA condition with a dose of 1.59 nC/ μ m² has an etch depth of ~65 nm and the corresponding SEM image has a smooth topology, indicative of the SiO₂ underlayer. At higher doses in the 0.025 nA series, the etching proceeds, albeit slower, into the SiO₂ layer (which can also be etched via FEBIE). The 0.1 nA etch progresses in an approximately linear

Nanoscale Horizons Page 10 of 25

fashion and the Nb film experiences some roughening during the FEBIE process, which manifests in the SEM images as higher brightness/grey scale in Fig. 2B) at 0.61 nC/μm². Figure 2C) is a sequence of linear fits (note log scale) from etch depth versus electron dose plots for a series of beam currents (see supplemental information Fig. S1-2 for higher current AFM and SEM images). Note that the etched volume as a function of areal dose increases with decreasing beam current. Figure 2D) is a plot of the average volumetric etch rate versus beam current (see supplemental information Fig. S3 for SEM images), where etch rate is the slope of the fitted lines in Fig. 2C), and illustrates that lower current yields lower etch rates, but higher volumetric etch efficiency. Also included in Fig. 2D) on the second y-axis is the volumetric etch efficiency, which is normalized to the electron dose.

While discussed in detail below, we qualitatively note that with increasing beam current we expect an eventual transition from an electron reaction limited regime to an XeF₂ mass transport limited regime. A full understanding of this transition between regimes necessitates an investigation of the effects of precursor pressure/flux. To this end, a second experiment was run at similar conditions but at a working pressure of 3x10⁻⁵ Torr and a beam current range of 0.1-1.6 nA, the results of which are also shown in **Fig. 2D**). Raising the pressure has the expected effect of increasing the etch rate and efficiency, and the proportional increase in general increases with increasing current. Interestingly, the volumetric etch rate is relatively constant for these conditions over the current range studied, while the volumetric etch efficiency decreases proportionally to the beam current. While we will discuss in the reaction kinetics in more detail in the discussion section, it is noteworthy that while the current increases a factor of 32x and 16x for the low- and high-pressure studies, respectively, the

efficiency decreases by a factor of ~100x and 16x. Again, we attribute these observations to a shift from low current limited by the electron stimulated reactions to limitations in mass transport of XeF_2 at the higher beam currents.

Based on the correlation between SEM images and AFM depth profiling, endpoint monitor (EPM) graphs of the concurrent SEM grey scale during the etching process were used to monitor the etching process. For this study a beam energy of 20 keV, dwell time of 0.025 μs, pixel pitch of 10 nm, and XeF₂ working pressure of 4.7x10⁻⁶ Torr were used. Etch experiments were conducted for a beam current range of 0.1-0.8 nA and EPM graphs and SEM images were used to infer the dose-to-clear the ~65 nm Nb film. Figure 3A) shows a series of EPM graphs for the 0.1 nA time series, which shows very good repeatability of the progressive salient features of the EPM graph. Inset are SEM captures taken at the associated doses in general, there is a slight decrease in the grey scale that we attribute to removal of the native NbO_x layer. Next, the grey scale increases due to slight roughening of the Nb film during etching, and reaches a maximum. After the maximum, the grey scale decreases as the underlying SiO₂ layer emerges and the inflection from the steep negative slope (denoted as an *) was determined to be the signature of the Nb film end point. Figure 3B) is a summary plot of the etch rate and efficiencies determined from the EPM graphs; for these conditions, the etch rate increases and the etch efficiency decreases with increasing current. Again, note that the current range studied here is a factor of 16x, while the etch rate efficiency changes by a factor of ~7.5x. The SEM images after etching and the associated EPM graphs can be found in supplemental information Fig. S4.

Nanoscale Horizons Page 12 of 25

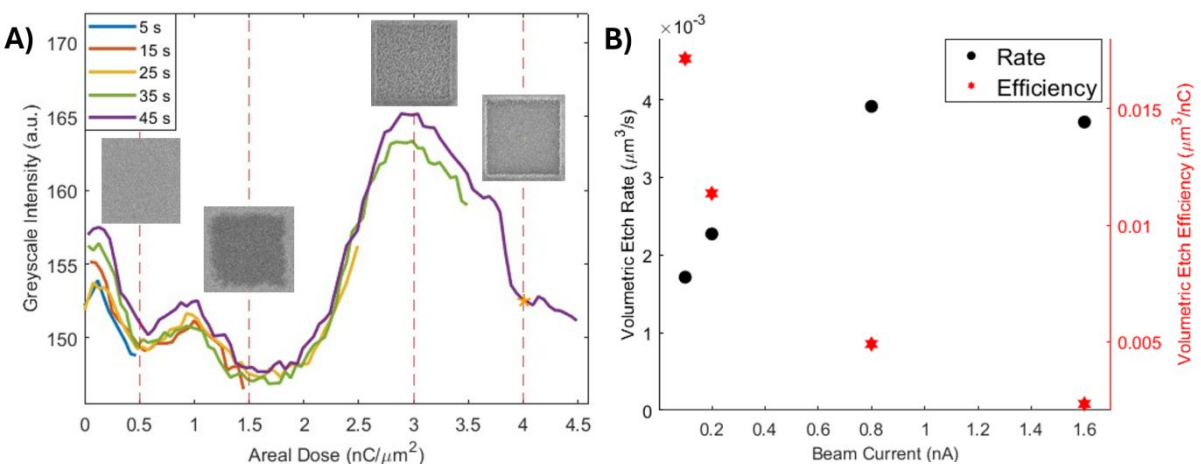


Figure 3. Gas-assisted FEBIE of 1 μm^2 box etches were conducted at a beam energy of 20 keV, 0.025 μ s dwell time, pixel pitch of 10 nm, and XeF₂ working pressure of 4.7x10⁻⁶ Torr and beam currents of 0.1, 0.2, 0.8 and 1.6 nA. A) illustrates a series of EPM graphs for FEBIE experiments run at 0.1 nA to various times (insets are SEM images taken at those dose/times. B) FEBIE volumetric etch rate (linear left Y axis) and etch efficiency (linear right Y axis) vs. beam current.

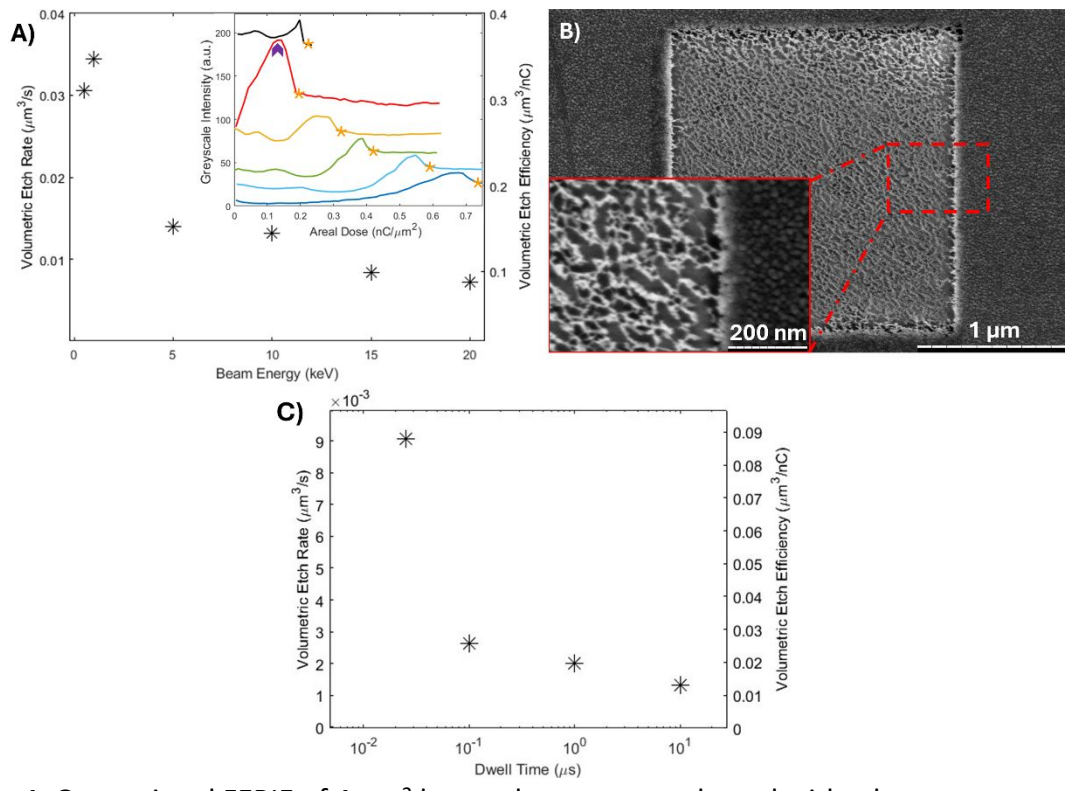


Figure 4. Gas-assisted FEBIE of 4 μ m² box etches were conducted with a beam current of 0.1 nA, dwell time of 0.025 μ s, pixel pitch of 10 nm, XeF₂ working pressure of 1x10⁻⁵ Torr, A) plot of beam energy vs FEBIE etch rate (left Y axis) and etch efficiency (right Y axis) where beam energies were varied from 0.5-20 keV, and inset is EPM graphs with dose to clear (all Nb removed) denoted by star for each voltage, B) SEM images of roughness

induced from non-cleared 5 second etch from the 1 keV series (marked on 1keV EPM by purple arrow, and inset is higher magnification image edge of box etch), and C) plot of dwell time vs FEBIE etch rate (left scale) and etch efficiency (right scale) for dwell times series at beam energy of 20 keV.

Next, the effect that beam energy and dwell time has on the gas-assisted FEBIE etching rate and efficiency was investigated. The box patterns were also increased to 4 μm² to increase the time needed to clear to better observe the etch evolution. For this study, a beam energy range of 0.5-20 keV was explored while parameters of a dwell time of 0.025 µs, pixel pitch of 10 nm, XeF₂ working pressure of 1x10⁻⁵ Torr, and abeam current of 0.1 nA were employed. **Figure 4A)** shows the volumetric etch rate and efficiency versus beam energy with the inset illustrating the EPM graphs (see associated SEM images and EPM graphs in supplemental information Fig. **S5**). Note, the EPM graphs have the same signatures regardless of beam energy. The Nb etching rate and efficiency (the same functionality because they were performed at just one current), increases slightly from 0.5 to 1 keV and then systematically decreases with increasing beam energy. This behavior illustrates an important aspect of the FEBIE process, namely, that the process is largely driven by the lower energy secondary electrons (specifically SE₁ type induced from the incident beam), which have a higher dissociation cross section for the adsorbed precursor.[35-38] Here, the trend suggests that the maximum in the SE yield is between 1 and 5 keV and the decrease in the etching rate observed with an increase in energy is attributed to the decrease in the secondary electron yield. Additionally, while the SE_{II} contribution at high beam energy is associated with a large interaction volume that results in an effectively low areal dose, SE_{II} electrons that result from low beam energy are associated with smaller interaction volumes and thus higher areal doses. Finally, simulations of focused electron beam induced deposition suggest that the primary beam energy contribution to the

Nanoscale Horizons Page 14 of 25

dissociation can be non-negligible and is also higher at lower beam energy. Summarily, the low beam energy peak in the volumetric etch efficiency is consistent with expectations. [35-38] Note, we deliberately used a low current and short dwell time to move our regime to an electron reaction rate limited to regime to better observe this energy dependence as will be shown below. Figure 4B) are SEM images taken at the peak of the EPM plot for the 1 keV series (dose = 0.125 nC/μm²). As evidenced by these images, the Nb-XeF₂ gas-assisted FEBIE process is not a uniform layer-by-layer etching process, but rather the etching occurs through the formation of nano-pores that coarsen until the films have been cleared. For the dwell time series, a range of dwell times from 0.025 to 10 µs was investigated at a beam energy 20 keV, beam current of 0.1 nA, pixel pitch of 10 nm, and XeF₂ working pressure of 1x10⁻⁵ Torr. Figure **4C)** shows that the FEBIE etch rate and efficiency increases dramatically from 0.025 to 0.1 µs and then more gradually at longer dwell times (see associated SEM images and EPM graphs in supplemental information Fig. S6). This transition is again a signature that at short dwell times, the exposed pixel has sufficient adsorbed XeF₂ molecules to be limited by the electron flux, but at longer dwell times, the adsorbed precursor is exhausted and subsequent transport via adsorption and diffusion limit the process.

3.2 Line etches

Next, single line etching for direct write patterning of niobium films was explored to determine the highest resolution lines that can be etched via FEBIE. **Figure 5** illustrates the results of a study that varied the XeF_2 pressure $1.04x10^{-6}$ to $1.15x10^{-5}$ Torr and etching a series of lines at similar conditions (20 keV, 0.1 nA, 0.025 μ s dwell time).

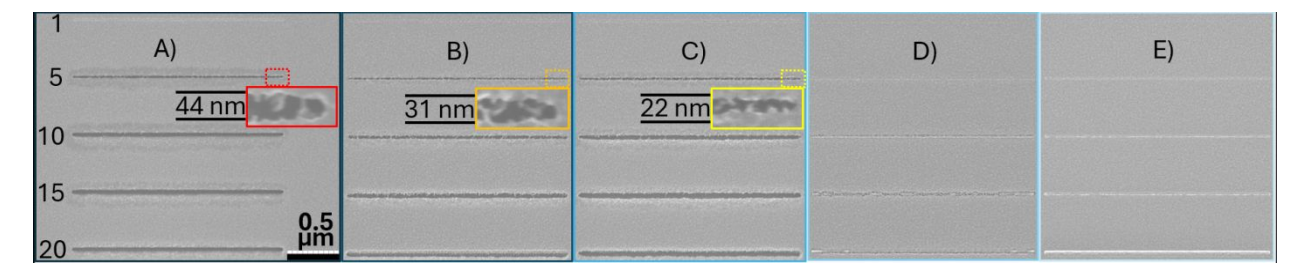


Figure 5. SEM images of 2 μ m long gas-assisted FEBIE line etches for an beam energy of 20 keV, beam current of 0.1 nA, dwell time of 0.025 μ s, pixel pitch of 10 nm, and varying XeF₂ working pressure; A) 1.15x10⁻⁵ Torr with inset of higher magnification of 5 second etch, B) 8.48x10⁻⁶ Torr with inset of higher magnification of 5 second etch, C) 5.93x10⁻⁶ Torr with inset of higher magnification of 5 second etch, D) 2.67x10⁻⁶ Torr, and E) 1.04x10⁻⁶ Torr.

First, we note that there is appreciable line edge roughness in the etches, which will ultimately affect the Josephson junction transport. This increase in working pressure resulted in the expected behavior of an increase in the etch rate. As noted in the high-resolution inset images, the etch line width of the 5 s lines increase with increasing pressure, which indicate that these are progressively over etched. An optimum resolution of 22 nm is achieved in the 5.93x10⁻⁶ Torr 5 second etch, though presumably comparable widths could be obtained at lower times for the higher pressures. We also note that in Fig. 5D) that the 15 s etch is etched slightly more than the 20 s etch; while we do not fully understand this anomaly, it could be associated with a spontaneous etching component as the 15 s etch was etched and was exposed to XeF₂ during the 20 s etch. While faster etching is preferable for larger features, good control of the time to clear is critical, thus slowing the etch by reducing the pressure slightly could be advantageous. For instance, spontaneous etching of the features during and post etching could be operative so that a reduction in precursor pressure could be leveraged to minimize this effect. We note that similar spontaneous etching was observed in TaON films, where passivation layers were reported to inhibit this behavior.^[20] Furthermore, recently Co-Si based materials were

Nanoscale Horizons Page 16 of 25

selectively oxidized via electron beam irradiation in H_2O .^[39] We hypothesize that similar passivation strategies may also be conducive to reducing spontaneous etching of Nb thin films and will explore this, as needed, in future works.

The effect of dwell time in the range of 0.025 - $100 \, \mu s$ was also investigated using patterning and gas flow parameters similar to the previous dataset ($20 \, keV$, $0.1 \, nA$, and XeF_2 working pressure of $4.7x10^{-6}$ Torr). Etch times were varied from 1- $20 \, s$ for each dwell time study. As illustrated in **Fig. 6**, the line patterns exhibited qualitatively higher etch rates for shorter dwell times and it appears that at long dwell times the FEBIE process is completely inhibited, similar to what was observed in FEBIE etching of Ti. [22-23] Similar to what was proposed for titanium, we speculate that the residence time of the volatile NbF₅ species could be long enough that at longer dwell times, subsequent re-dissociation of NbF₅ towards to NbF₄ products could occur. NbF₄ is a non-volatile solid and thus the long dwell time promotes a desorption limited regime.

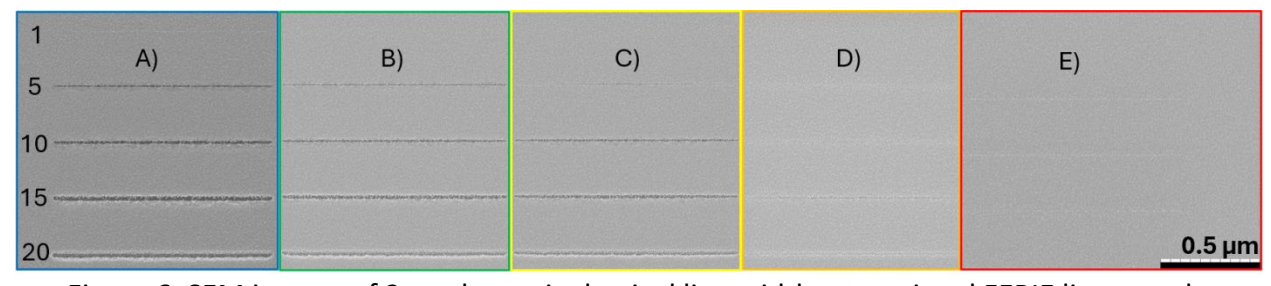


Figure 6. SEM images of 2 μ m-long, single pixel line width gas-assisted FEBIE lines at a beam energy of 20 keV, current of 0.1 nA, pixel pitch of 10 nm, XeF₂ working pressure of 4.7x10⁻⁶ Torr, and total times from 1-20 s, for dwell times of A) 0.025, B) 0.1, C), 1, D) 10, and E) 100 μ s.

Finally, **Fig. 7** compares a FEBIE series at 20 keV and 0.5 keV (0.1 nA, 0.025 μ s, and 1x10⁻⁵ Torr XeF₂). As illustrated, the 20 keV lines look qualitatively similar to those produced using the highest working pressure (see **Fig. 5**). High magnification images of the 1 s and 2.5 s lines reveal an approximate line width of 17 nm and 30 nm, respectively.

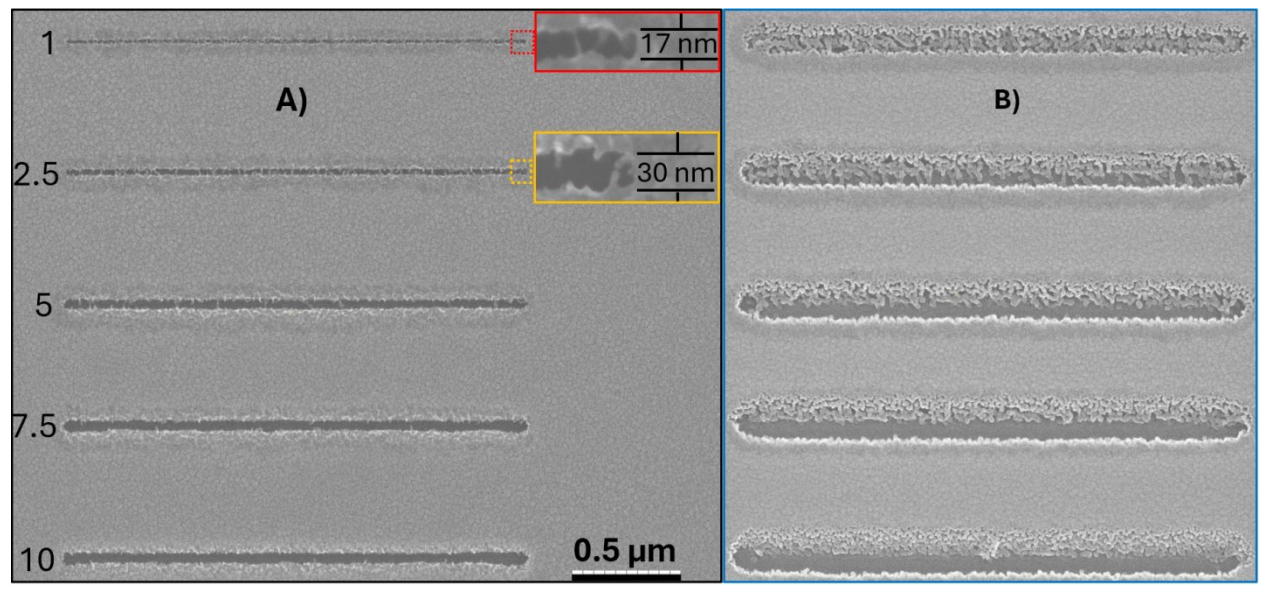


Figure 7. SEM images of 2 μ m single pixel linewidth gas-assisted FEBIE lines at a beam current of 0.1 nA, dwell time of 0.025 μ s, pixel pitch of 10 nm, XeF₂ working pressure of 1x10⁻⁵ Torr at beam energies of A) 20 keV with higher magnification images showing thicknesses of 1 and 2.5 second etches, and B) 0.5 keV.

At the 0.5 keV beam energy the line widths increase, which is likely due to the highly localized electron interaction volume and etch contributions from SE_{II} electrons generated from backscattered electrons. Interestingly, the bottom half of the line clears faster than the top half, which we believe is evidence for charging and subsequent beam drift during the line etch such that charge mitigation strategies for low voltage etching will need to be explored.

4. Discussion

To understand the various etch rate and efficiency results and distinguish the electron beam stimulated and mass transport limited regimes, it is instructive to understand the relative gas flux and electron flux as well as the cumulative electron dose realized during the electron beam dwell time. For context, all the experiments were run with a 10 nm pixel pitch in the x-y raster scan modes, so we can normalize everything to a nominal 100 nm² area for each pixel addressed. Clearly, this is not a full description of the physics as this does not account for

Nanoscale Horizons Page 18 of 25

variations in beam diameter and interaction volumes as we change beam conditions. However, we will discuss these effects in the context of how they cause deviations from expected behavior of a nominal 100 nm^2 exposure pixel. **Table I** lists the various experimental conditions along with the localized precursor and electron flux, and cumulative electron dose per pixel for a single dwell time. The estimated number of XeF₂ monolayers that impinge during the scan/refresh time (product of the number of pixels and per pixel dwell time) is also listed, as well as the ratio of the number of electrons per dwell to the number of XeF₂ gas sites occupied, both normalized to a 100 nm^2 pixel; we assume a Langmuir isotherm for XeF₂ on Nb, thus for conditions where the number of monolayers impinged is greater than 1, the coverage is assumed to be unity (or $\sim 11.8 \text{ XeF}_2/\text{nm}^2$ or $1180 \text{ XeF}_2/\text{pixel}$). Finally, the Nb etch efficiency (Nb atoms etched/e') is included in the table, which is determined from the dose-to-clear (all Nb removed), the effective volume of the Nb etched (box size x thickness), and assumes a theoretical Nb density of 8.58 g/cm^3 . Note that overall, the etching efficiency is high and in some experiments exceeds unity.

Table I. Summary etch statistics for all box etch experiments.

#	Conditions	Gas flux (XeF ₂ /nm ² s) ×10 ⁴	Electron flux (e ⁻ /pixel-s) ×10 ⁸	Electron Areal Dose per pixel area, per dwell (e ⁻ /100 nm ²)	XeF ₂ monolayers per refresh	Flux Ratio e- /XeF2 x10-1	Nb atoms etched/e
1	0.025 nA 1keV 1us 1x10 ⁻⁵	2.32	1.56	156.1	19.6	1.32	1.59
2	0.1 nA 1keV 1us 1x10 ⁻⁵	2.32	6.24	624.2	19.6	5.29	0.38
3	0.2 nA 1keV 1us 1x10 ⁻⁵	2.32	12.5	1248.4	19.6	10.6	0.11
4	0.4nA 1keV 1us 1x10 ⁻⁵	2.32	25.0	2496.9	19.6	21.2	0.06
5	0.8nA 1keV 1us 1x10 ⁻⁵	2.32	49.9	4993.8	19.6	42.3	0.02
6	0.1 nA 1keV 1us 3x10 ⁻⁵	6.95	6.24	624.2	58.9	5.29	1.35
7	0.2 nA 1keV 1us 3x10 ⁻⁵	6.95	12.5	1248.4	58.9	10.6	0.76

8	0.4nA 1keV 1us 3x10 ⁻⁵	6.95	25.0	2496.9	58.9	21.2	0.34
9	0.8 nA 1keV 1us 3x10 ⁻⁵	6.95	49.9	4993.8	58.9	42.3	0.22
10	1.6 nA 1keV 1us 3x10 ⁻⁵	6.95	99.9	9987.5	58.9	84.6	0.08
11	0.1 nA 20keV 25ns 4.7x10 ⁻⁶	1.09	6.24	15.6	0.2	0.57	0.15
12	0.2 nA 20keV 25ns 4.7x10 ⁻⁶	1.09	12.5	31.2	0.2	1.15	0.10
13	0.8 nA 20keV 25ns 4.7x10 ⁻⁶	1.09	49.9	124.8	0.2	4.58	0.04
14	1.6 nA 20keV 25ns 4.7x10 ⁻⁶	1.09	99.9	249.7	0.2	9.17	0.02
15	0.1 nA 20keV 25ns 1x10 ⁻⁵	2.32	6.24	15.6	2.0	0.13	0.78
16	0.1 nA 20keV 0.1us 1x10 ⁻⁵	2.32	6.24	62.4	7.9	0.53	0.23
17	0.1 nA 20keV <i>1us</i> 1x10 ⁻⁵	2.32	6.24	624.2	78.6	5.29	0.17
18	0.1 nA 20keV 10us 1x10 ⁻⁵	2.32	6.24	6242.2	785.8	52.9	0.12
19	0.1 nA 0.5keV 25ns 1x10 ⁻⁵	2.32	6.24	15.6	2.0	0.13	2.76
20	0.1 nA 1keV 25ns 1x10 ⁻⁵	2.32	6.24	15.6	2.0	0.13	3.09
21	0.1 nA <i>5keV</i> 25ns 1x10 ⁻⁵	2.32	6.24	15.6	2.0	0.13	1.36
22	0.1 nA 10keV 25ns 1x10 ⁻⁵	2.32	6.24	15.6	2.0	0.13	1.29
23	0.1 nA 15keV 25ns 1x10 ⁻⁵	2.32	6.24	15.6	2.0	0.13	0.88
24	0.1 nA 20keV 25ns 1x10 ⁻⁵	2.32	6.24	15.6	2.0	0.13	0.78

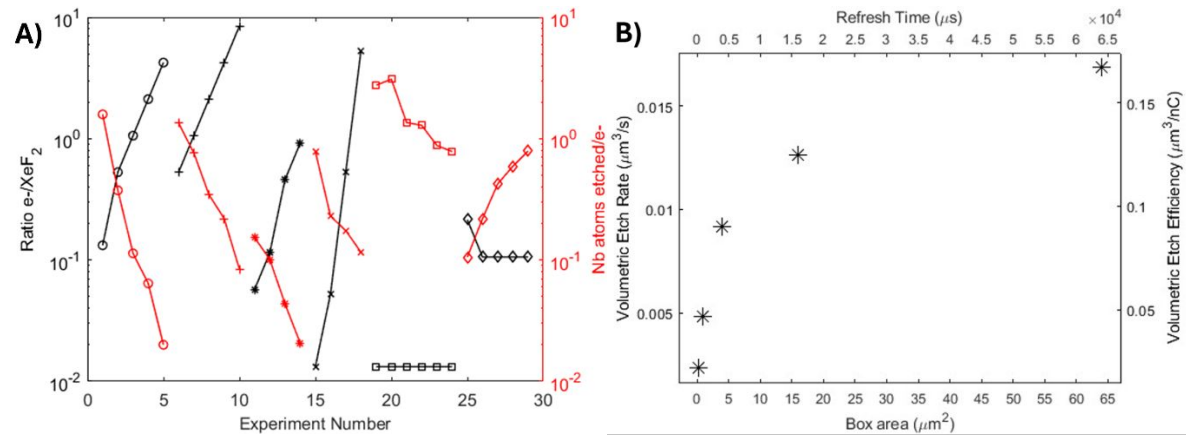


Figure 8. A) Summary plot of the ratio of e-/XeF₂ (left y-axis) and Nb atoms etched per electron (right y-axis) of box etch experiments from Table I. B) FEBIE volumetric etch rate (left y axis) and volumetric etch efficiency (right y-axis) as a function of area (bottom x-axis) and refresh time (top x-axis).

Figure 8A) is a plot of the ratio of the number of electrons per dwell to the number of XeF_2 gas sites occupied for each box etch experiment and the corresponding Nb etch efficiency. As expected, there is a strong correlation between increasing the e^-/XeF_2 ratio and decreasing Nb

atom per electron etch efficiency. This suggests that while some experimental conditions have an equilibrium surface coverage at the beginning of the pixel dwell, the refresh of XeF₂ precursor during the pixel exposure is slow relative to the pixel dwell time, and thus the Nb etch efficiency decreases as the surface concentration decreases during the pixel exposure. This effect is most prominent at high current and long dwell time. Interestingly, the dwell time experiment has the poorest correlation of the two slopes. Note that the negative slope of the Nb atom/ e^- is less steep and changes slope relative to the e^- /XeF₂ ratio, which possibly suggests a secondary mechanism is operative. We attribute the change in slope at longer dwell times in this experiment to spontaneous etching that is occurring. To test this, we performed an experiment at 20 keV beam energy, 0.2 nA current, 0.1 μs dwell time and 1x10⁻⁵ Torr XeF₂ working chamber pressure with increasing box area (0.25-64 μm²) (see Table SII for tabulated data); this effectively increases the time for spontaneous etching to occur while holding the electron stimulated contribution constant. As observed in Fig. 8B), the Nb volumetric etch rate (and efficiency) increases with increasing box area, which confirms that during the cumulative refresh time (secondary x-axis), the Nb film experiences spontaneous etching; if no spontaneous etching occurred, the volumetric etch efficiency should be constant with area. Interestingly, the slope is not constant, thus the spontaneous etching contribution is not constant, but seems to decrease with increasing area. The details of the spontaneous etching contribution will be explored in more detail in future work.

Conclusions

The impact of varying beam current, dwell time, beam energy, XeF₂ working pressure, and spontaneous etching were found for the FEBIE of Nb films. Lower beam current, low dwell

Page 21 of 25

time and higher XeF₂ working chamber pressure increase the Nb etch efficiency and values as high as 3 Nb atoms/e-. Calculations of the relative electron and localized gas flux were used to elucidate the electron stimulated reaction rate and mass transport limitation contributions to the process. The observed behavior is attributed to XeF₂ gas depletion as the dose per pixel increases as gas replenishment during the pixel dwell is negligible. Additionally, non-linearities in the etching efficiency at long dwell times suggested that a spontaneous etching component was also contributing. Area-dependent etching experiments in which all the beam and precursor parameters are constant, confirmed that spontaneous etching contributes to the etching process, thus judicious scanning parameters need to be considered when employing this process. The etch efficiency as a function of beam energy was determined to achieve a maximum at 1 keV, which correlates to the range in which the secondary electron yield is highest as would be expected in an SE_I and SE_{II} dominated reaction pathway. Optimal FEBIE parameters were explored and an etched line width of ~17 nm was demonstrated, which is well within range of the superconducting coherence length of Nb, and should offer an intriguing option for direct write fabrication of Josephson junctions and other superconducting devices.

Author contributions

Spencer Gellerup: FEBIE experiments, SEM Imaging, AFM, manuscript preparation

Reece Emery: Nb sputtering synthesis

Scott T. Retterer: Project and funding management, manuscript review

Steven J. Randolph: Experimental Design, manuscript preparation and review

Philip D. Rack: Experimental design, program supervision, manuscript preparation and review

Nanoscale Horizons Page 22 of 25

Conflicts of interest

The authors declare no competing financial interest.

Acknowledgments

All research was performed at the Center for Nanophase Materials Sciences, which is a U.S. Department of Energy Office of Science user facility at Oak Ridge National Laboratory (ORNL) which is managed by UT-Battelle, LLC, for the U.S. Department of Energy. The authors would like to thank Dr. John Lasseter of the ORNL Center for Nanophase Materials Sciences for producing Figure 1A) of this work.

References

- [1] P. Das, C.V. Tomy, S.S. Banerjee, H. Takeya, S. Ramakrishnan, and A.K. Grover, *Phys. Rev. B*, 2008, **78**, 214504. https://doi.org/10.1103/PhysRevB.78.214504
- [2] R. Prozorov, M. Zarea, and J.A. Sauls, *Phys. Rev. B*, 2022, **106**, L180505. https://doi.org/10.1103/PhysRevB.106.L180505\
- [3] J. Guo, G.C. Lin, S. Cai, C.Y. Xi, C.J. Zhang, W.S. Sun, Q.L. Wang, K. Yang, A.G. Li, Q. Wu, Y.H. Zhang, T. Xiang, R.J. Cava, and L.L. Sun, *Adv. Mater.*, 2019, **31**, 1807240. https://doi.org/10.1002/adma.201807240
- [4] J.F. Smith and O.N. Carlson, *Bull. of Alloy Phase Diagrams*, 1983, **4**, 46–49. https://doi.org/10.1007/BF02880319
- [5] J.R. Gavaler, Appl. Phys. Lett., 1973, 23, 480–482. https://doi.org/10.1063/1.1654966
- [6] A. Godeke, A. den Ouden, A. Nijhuis, and H.H.J. ten Kate, *Cryogenics*, 2008, **48**, 308-316. https://doi.org/10.1016/j.cryogenics.2008.04.003.
- [7] J.R. Hopkins and D. K. Finnemore, *Phys. Rev. B*, 1974, **9**, 108. https://doi.org/10.1103/PhysRevB.9.108
- [8] H. Tian, C.E. Reece, M.J. Kelley, S. Wang, L. Plucinski, K.E. Smith, and M.M. Nowell, *Appl. Surf. Sci.*, 2006, **253**, 1236-1242. https://doi.org/10.1016/j.apsusc.2006.01.083
- [9] M.V. Altoe, A. Banerjee, C. Berk, A. Hajr, A. Schwartzberg, C. Song, M. Alghadeer, S. Aloni, M. Elowson, J.M. Kreikebaum, E. Wong, S. Griffin, S. Rao, A. Weber-Bargioni, A. Minor, D. Santiago, S. Cabrini, I. Siddiqi, and D. Ogletree, *PRX Quantum*, 2022, **3**, 020312. 020312.10.1103/PRXQuantum.3.020312

- [10] A. Anferov, K.H. Lee, F. Zhao, J. Simon, and D.I. Schuster, *Phys. Rev. Applied*, 2024, **21**, 024047. https://doi.org/10.1103/PhysRevApplied.21.024047
- [11] C.W. Johnson, A.K. Schmid, M. Mankos, R. Röpke, N. Kerker, I.S. Hwang, E.K. Wong, D.F. Ogletree, A.M. Minor, and A. Stibor. *Phys. Rev. Applied*, 2023, **19**, 034036. https://doi.org/10.1103/PhysRevApplied.19.034036
- [12] W. DeSorbo, Phys. Rev., 1963, 132, 107. https://doi.org/10.1103/PhysRev.132.107
- [13] S. Balachandran, A. Polyanskii, S. Chetri, P. Dhakal, Y.F. Su, Z.H. Sung, and P.J. Lee, *Sci. Rep.*, 2021, **11**, 5364. https://doi.org/10.1038/s41598-021-84498-x
- [14] K.T. Mahady, S. Tan, Y. Greenzweig, A. Raveh, and P.D. Rack, Nanoscale Advances, 2019, **1**, 3584-3596. https://doi.org/10.1039/C9NA00390H
- [15] S. Wang, Y.M. Sun, J.M. White, A. Stivers, and T. Liang, *J. Vac. Sci. Technol. B*, 2005, **23**, 206–209. https://doi.org/10.1116/1.1848107
- [16] T. Bret, B. Afra, R. Becker, T. Hofmann, K. Edinger, T. Liang, and P. Hoffmann, *J. Vac. Sci. Technol. B*, 2009, **27**, 2727–2731. https://doi.org/10.1116/1.3243208
- [17] M.G. Stanford, K. Mahady, B.B. Lewis, J.D. Fowlkes, S. Tan, R. Livengood, G.A. Magel, T.M. Moore, and P.D. Rack, *ACS Appl. Mater. Interfaces*, 2016, **8**, 29155–29162. https://doi.org/10.1021/acsami.6b09758
- [18] S.J. Randolph, M. Toth, J. Cullen, C. Chandler, and C. Lobo, *Appl. Phys. Lett.*, 2011, **99**, 21310. https://doi-org.utk.idm.oclc.org/10.1063/1.3662928
- [19] M. Yemini, B. Hadad, Y. Liebes, A. Goldner, and N. Ashkenasy, *Nanotechnology*, 2009, **20**, 245302. DOI 10.1088/0957-4484/20/24/245302
- [20] M.G. Lassiter, T. Liang, P.D. Rack, J. Vac. Sci. Technol. B, 2008, 26, 963–967. https://doi.org/10.1116/1.2917076
- [21] A. Ganczarczyk, M. Geller, and A. Lorke, *Nanotechnology*, 2011, **22**, 045301. Doi: 10.1088/0957-4484/22/4/045301.
- [22] F.J. Schoenaker, R. Córdoba, R. Fernández-Pacheco, C. Magén, O. Stéphan, C. Zuriaga-Monroy, M.R. Ibarra, and J.M. De Teresa, *Nanotechnology*, 2011, **22**, 265304. doi:10.1088/0957-4484/22/26/265304
- [23] J.H. Noh, J. D. Fowlkes, R. Timilsina, M.G. Stanford, B.B. Lewis, and P.D. Rack, *ACS Appl. Mater. Interfaces*, 2015, **7**, 4179–4184. https://doi.org/10.1021/am508443s
- [24] J. Wang, D.P. Griffis, R. Garcia, and P.E. Russell, *Semicond. Sci. Technol.*, 2003, **18**, 199. https://doi.org/10.1116/1.1848107
- [25] J. Lasseter, S. Gellerup, S. Ghosh, S.J. Yun, R. Vasudevan, R.R. Unocic, O. Olunloyo, S.T. Retterer, K. Xiao, S.J. Randolph, and P.D. Rack, *ACS Appl. Mater. Interfaces*, 2024, **16**, 9144–9154. https://doi.org/10.1021/acsami.3c17182

- [26] F. Fairbrother and W.C. Frith, J. Chem. Soc., 1951, **675**, 3051-3056.
- [27] J.H. Junkins, R.L. Farrar Jr, E.J. Barber, and H.A. Bernhardt, *J. Am. Chem. Soc.*, 1952, 74, 3464-3466.
- [28] F. Fairbrother, K. H. Grundy, and A. Thompson J. Chem. Soc., 1965, **121**, 761-765.
- [29] K. M. Alexander and F. Fairbrother, J. Chem. Soc., 1949, 48, 223-227.
- [30] F. Fairbrother, The Chemistry of Niobium and Tantalum, Elsevier, London, 1967.
- [31] T.T. Foxe, B.D. Hunt, C. Rogers, A.W. Kleinsasser, and R.A. Buhrman, *J. Vac. Sci. Technol.*, 1981, **19**, 1394–1397. https://doi.org/10.1116/1.571217
- [32] K.T. Kohlmann, M. Thiemann, and W.H. Brünger, *Microelectron. Eng.*, **13**, 1991, 279-282, https://doi.org/10.1016/0167-9317(91)90093-S
- [33] V. Friedli and I. Utke, *J. Phys. D: Appl. Phys.*, 2009, **42**, 125305. DOI 10.1088/0022-3727/42/12/125305
- [34] R. Winkler, J. Fowlkes, A. Szkudlarek, I. Utke, P.D. Rack, and H. Plank, *ACS Appl. Mater. Interfaces*, 2014, **6**, 2987–2995. https://doi.org/10.1021/am405591d
- [35] D.A. Smith, J.D. Fowlkes, and P.D. Rack, *Nanotechnology*, 2007, 18, 265308.
- [36] D.A. Smith, J.D. Fowlkes, and P.D. Rack, Nanotechnology 2008, 19, 415704.
- [37] D.A. Smith, J.D. Fowlkes, and P.D. Rack, Small, 2008, 9, 1382.
- [38] J.D. Fowlkes, S.J. Randolph, and P.D. Rack, J. Vac. Sci. Technol. B, 2005, 23, 2825.
- [39] S. Barth, F. Porrati, D. Knez, F. Jungwirth, N.P. Jochmann, M. Huth, R. Winkler, H. Plank, I. Graciae and C. Canée, Nanoscale, 2024, **16**, 14722-14729.

- All data for this communications article was created by me, Spencer Gellerup, using the facilities in the Center for Nanophase Materials Science at Oak Ridge National Laboratory
- The data supporting this article is included in the main text as well as in the Supplementary Information.